AIAA JOURNAL
Vol. 35, No. 4, April 1997

# Effects of Internal Nozzle Geometry on Compression-Ramp Mixing in Supersonic Flow

Yaacov Haimovitch,* Ehud Gartenberg,† and A. Sidney Roberts Jr.‡
*Old Dominion University, Norfolk, Virginia 23529-0247*
and
G. Burton Northam§
*NASA Langley Research Center, Hampton, Virginia 23681*

**An experimental study based on flow visualization has been conducted in a constant-area duct fitted with a swept-ramp fuel injector to explore mixing enhancement techniques for supersonic combustion ramjet (scramjet) engines. The main flow was air at Mach 2, and the hydrogen fuel was simulated by helium injected at Mach 1.70 and by air injected at Mach 1.63. Mie scattering from ethanol-seeded helium or air was used to visualize the simulated fuel flow injected into the main airstream. Six injector nozzle inserts for preconditioning the simulated fuel jet were tested to explore its interaction with the vortical flow produced by the ramp. The six nozzle inserts were as follows: circular nozzle (baseline), nozzle with three downstream facing steps in the divergent section, nozzle with four vortex generators, elliptical nozzle, tapered-throat nozzle, and trapezoidal nozzle. Mixing characteristics of the different inserts were inferred from image analysis. The results indicate that the mixing process is dominated by the ramp-generated vorticity, the injectors' inner geometry having a secondary effect. It also was found that the simulated fuel–air mixing in the far field is nearly independent of the injector geometry, molecular weight of the injected gas, and the initial convective Mach number.**

## Nomenclature

| | |
|---|---|
| $A$ | = area |
| $a$ | = speed of sound |
| $d$ | = injector exit diameter |
| $h$ | = ramp base height |
| $L$ | = length |
| $M$ | = Mach number |
| $\dot{m}$ | = mass flow rate |
| $P$ | = perimeter |
| $p$ | = pressure |
| $Re$ | = Reynolds number |
| $Sc$ | = Schmidt number |
| $T$ | = temperature |
| $U$ | = velocity |
| $x$ | = streamwise, axial coordinate |
| $y$ | = cross-stream coordinate |
| $z$ | = vertical coordinate |
| $\delta$ | = shear-layer width |
| $\lambda_B$ | = Batchelor's scale (diffusion microscale) |
| $\rho$ | = density |
| $\tau_B$ | = Batchelor's timescale |

*Subscripts*

| | |
|---|---|
| $C$ | = convective |
| $d$ | = based on jet exit diameter |
| $e$ | = exit |
| $t$ | = throat |
| 0 | = stagnation |
| 1 | = high-velocity flow |
| 2 | = low-velocity flow |

Presented as Paper 94-2940 at the AIAA/ASME/SAE/ASEE 30th Joint Propulsion Conference, Indianapolis, IN, June 27–29, 1994; received Nov. 26, 1994; revision received Nov. 27, 1996; accepted for publication Jan. 8, 1997. 

*Doctoral Student, Department of Mechanical Engineering; currently Research Engineer, RAFAEL, Ministry of Defense, P.O. Box 2250, Dept. 46, Haifa 31021, Israel. Senior Member AIAA.
†Research Associate Professor, Department of Mechanical Engineering. Associate Fellow AIAA.
‡Professor, Department of Mechanical Engineering.
§Senior Research Scientist, Hypersonic Airbreathing Propulsion Branch, M.S. 197. Member AIAA.

## Introduction

SUPERSONIC combustion ramjet (scramjet) engines require enhanced mixing between the fuel and the air because of low shear-induced mixing typical of supersonic streams,[1] extremely short combustor residence time, overall sensitivity of the vehicle to the combustor size, and the requirement to extract thrust from the heated fuel injection[2] by maximizing its streamwise component. Therefore, mixing enhancement constitutes a very important factor in the design of scramjet engines. Three categories of injection methods have been investigated to produce the required mixing[3]:

1) Conditioning of the main flow by varying the injector/combustor wall geometry. These techniques are known as contoured wall injectors, e.g., ramp injectors and stepped combustor walls.

2) Preconditioning of the fuel through various turbulence and vorticity-generating devices within the injectors themselves, including noncircular nozzles.

3) Direct interaction between the fuel jet and the main flow. Shocks and expansion waves, which are inherent features of the flowfield, are used to generate instabilities and, subsequently, large-scale flow structures in the interface region. This category includes normal and angular injection from flat combustor walls.

The present work combines two techniques: the contoured wall injector based on a swept ramp and preconditioning of the fuel jet through various nozzle designs. Ramp injection was studied extensively at NASA Langley Research Center.[4–12] These injectors generate vorticity when incoming air is compressed by the top of the ramp and spills over the ramp corners into the lower-pressure region between the ramps. The effect is enhanced by sweeping the ramp side walls so that the region between the ramps diverges streamwise, causing the air in between to accelerate and expand to a lower pressure. The jet, injected at the ramp's base, is highly deformed by these vortices and lifted into two counter-rotating cores. In the case of the swept side-wall ramp, the mixing is augmented in comparison with the straight wall ramp and requires a shorter mixing length. However, the swept-ramp causes higher total pressure loss than the straight ramp. Another possibility for enhancing mixing is preconditioning the fuel flow through various

turbulence-enhancing and vorticity-generating devices within the injectors themselves. Several techniques have been explored, including noncircular nozzles. The elliptic and rectangular jets displayed greater spreading rates, especially in the minor axis plane, and a better overall mixing performance relative to the circular jets. The higher spreading is accompanied by a faster decay of the mean velocity along the jet axis and amplification of turbulent small-scale fluctuations.[13] The last effect also was observed in noncircular nozzles with corners, e.g., triangles, rectangles, or squares, where axial vortices are formed at the corners of the nozzles.[14] Cold flow tests made by Schadow et al.[15] with a circular nozzle having several downstream steps showed that the turbulence levels increased up to six times relative to a circular nozzle. Samimy et al.[16,17] and Zaman et al.[18] used tabs protruding into the flow at the exit plane of the nozzle, to generate vortices that distort the jet cross section and increase substantially the entrainment region. Gutmark et al.[19] studied the performance of a jet injected from a supersonic tapered-slot nozzle and observed a larger spreading along the minor axis of the slot. The turbulence intensity level is lower at the center, but it was uniformly distributed across the jet, with the highest relative intensity concentrated in the shear layer of the jet.

The reviewed results suggest that some combination of mixing methods is likely to produce the required mixing enhancement for a supersonic combustor with only a minimum loss in total pressure. In particular, a swept-ramp injector fitted with a fuel preconditioning device could couple the augmented vorticity of the supersonic main stream with the nearly parallel preconditioned fuel jet. The effectiveness of this design to enhance supersonic mixing was investigated in this study experimentally using Mie scattering of the seeded fuel jet.

## Experimental System

### Test Facility

The tests were conducted in the Transverse Jet Facility at NASA Langley Research Center, an open-loop blowdown facility with a rectangular Mach 2 convergent–divergent nozzle section. A rectangular cross-section duct assembly was connected at the nozzle exit. The duct had a uniform and constant cross section of 38.6 mm (1.52 in.) by 87.9 mm (3.46 in.). The planes of visualization were at the exit of the duct, perpendicular to its axis. Visualization at different cross sections downstream of the injection plane was performed by inserting duct extensions in steps of 50.8 mm (2 in.), from 114.3 mm (4.5 in.) up to 266.7 mm (10.5 in.) in total length.

### Injector Model

The injector model shown in Fig. 1 had one swept ramp located in the middle of the duct. The top wall of the ramp was inclined 10.3 deg relative to the duct wall. The side walls of the ramp were swept back 10 deg relative to the main flow, which was parallel to the duct walls. The ramp ended in a nearly square base 17.4 mm (0.685 in.) wide by 16.2 mm (0.639 in.) high. On both sides of the middle ramp, a portion of the side walls was swept to simulate the presence of adjacent ramps. The middle ramp was equipped with an injector connected to the "fuel" supply system. The injection angle was 10.3 deg relative to the main flow.

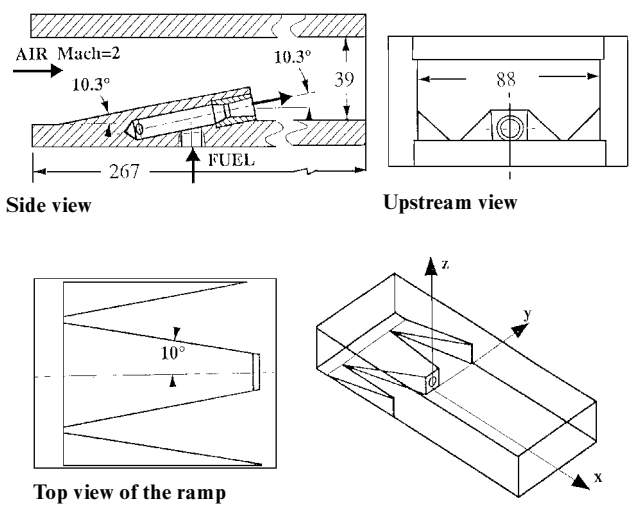


**Fig. 1 Schematic of injector model. Dimensions are in millimeters.**

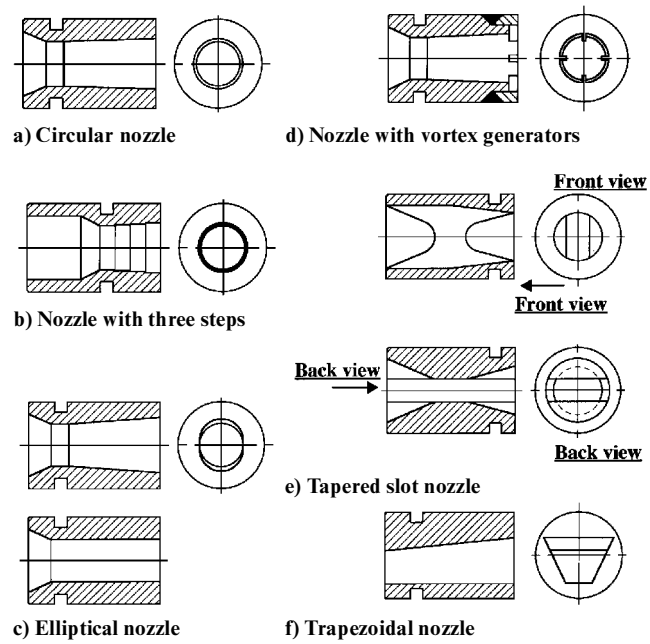


**Fig. 2 Injector-nozzle inserts for all nozzles: $Ae/At = 1.272$.**

### Injector-Nozzle Inserts

Six different nozzle inserts, shown in Fig. 2, were fabricated separately and then installed successively into the ramp. All of the nozzles had identical throat and exit areas, the ratio being $A/A^* = 1.272 \pm 0.040$; hence, they had essentially the same mass flow rate and exit Mach number. The six nozzle inserts were as follows:

a) Circular nozzle, used as the baseline configuration, had a throat diameter of 6.35 mm (0.250 in.) and an exit cross-section diameter of 7.16 mm (0.282 in.).

b) Circular nozzle with three downstream facing steps had a circular cross section with three downstream-facing steps in the divergent section, each having a length-to-step ratio of 16. These steps were supposed to enhance the small-scale turbulence.

c) Elliptical nozzle had a divergent section with an aspect ratio of 1.2. An elliptical nozzle spreads faster in the minor axis plane than in the major axis plane. The faster spread is accompanied by a faster decay of the mean velocity along the jet axis and an amplification of small-scale turbulent fluctuations. This nozzle was tested with the major axis parallel and perpendicular to the bottom wall.

d) Nozzle with four vortex generators, a circular conical nozzle with four vortex generators in the exit plane, corresponding to a maximum area blockage of about 5%. The vortex generators were rectangular tabs projecting normally into the jet. The tabs were intended to distort the jet cross section and to increase the mixing/entrainment area. This insert was tested with the tabs in cross orientation and with the tabs in X orientation relative to the bottom wall.

e) Tapered-throat nozzle with a 2.8:1 rectangular throat that blends smoothly into the diverging section leading to a circular exit. A supersonic tapered-throat nozzle spreads faster in the minor axis plane than in the major axis plane, and the vorticity generated by the nozzle's internal geometry augments the turbulence. The insert was tested with the throat's slot parallel and perpendicular to the bottom wall.

f) Trapezoidal nozzle was designed to generate axial vortices at the nozzle's corners, producing a significant amplification of small-scale turbulent fluctuations.

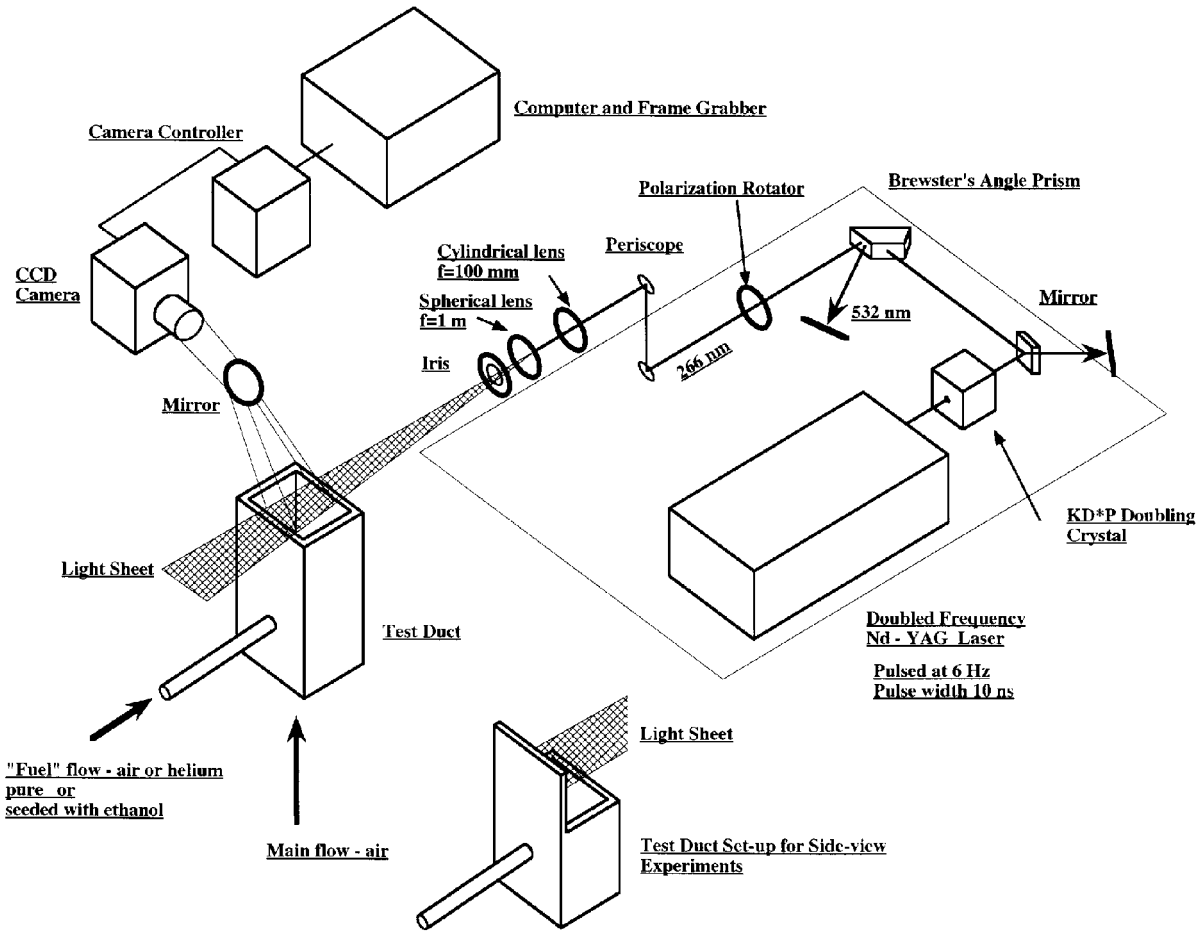


**Fig. 3 Mie-scattering optical arrangement.**

### Imaging System

*Laser System*

The optical arrangement of the imaging system is shown in Fig. 3. The illumination source was a frequency-doubled Nd:YAG laser, which was doubled again to a wavelength of 266 nm in the uv, using a temperature-phase-matched potassium diphosphate (KD*P) crystal mounted in a temperature-stabilized dry cell. The second doubling of the frequency was aimed at minimizing the light scattering of small particles that are naturally present in the main airflow, which was unacceptably large at 532 nm, but became acceptable at 266 nm (Ref. 20). The laser was pulsed at 6 Hz for bursts of 10 ns each. The uv light was split from the residual green with a Brewster's angle prism, and the plane of polarization was rotated with a quartz zero-order half-wave plate. The light sheet was formed by a pair of lenses: a plano–concave cylindrical lens with a focal length of 100 mm and a plano–convex spherical lens with a focal length of 1 m. Optics were uv-grade fused silica, coated for 266 nm. The theoretical thickness (diffraction limited) of the light sheet was about 0.05 mm; however, in practice the light sheet was thicker, about 0.5 mm at the waist. The spherical and cylindrical lenses were mounted on a rail that allowed the light sheet to be formed and moved to any position.

*Camera*

The images were recorded with an intensified video charge-coupled device (CCD) camera with 105-mm focal length $f/4.5$ lens. The CCD array had $512 \times 512$ sensing elements of $20 \times 20 \mu$m, each. The images were binned at a factor of 2, resulting in images of only $256 \times 256$ pixels. Binning is a technique of combining charges from adjacent pixels during the readout process. Because the spatial resolution was limited by the laser sheet, the binning increases the readout rate at no loss in the effective spatial resolution. The camera system was connected to a personal computer equipped with a frame grabber. The images were composed of 16-bit data (65,536 gray levels) and were digitized at a rate of 40,000 pixels/s with a digitization noise of 4 electrons rms. The camera exposure time was set to 167 ms to ensure the capture of a single laser pulse. In each case, a sequence of 10 single images was acquired and stored on the computer. The camera could be moved on a rail to any desired position.

### Experimental Conditions

The unheated airflow from the duct was discharged into the room. Throughout the test, the operating conditions were: total pressure $p_0 = 793 \pm 3$ kPa and total temperature $T_0$ equal to the ambient temperature. The fuel was simulated by helium or air. The fuel was seeded with ethanol for visualization. The ethanol was injected by pressurizing its supply tank with nitrogen at a pressure of 690 kPa higher than the pressure of the injected fuel. The ethanol flow rate was regulated with a fine-needle valve. An ample length of pipe ($\approx$20 m) with several elbows ensured evaporation and mixing ahead of the injector nozzle. The ethanol condensed upon expansion in the nozzle and provided Mie-scattering particles. The experimental conditions are summarized in Table 1, together with the shear-layer parameters. Following Papamoschou and Roshko,[1] $U_C$ is expressed in the form of a speed-of-sound weighted average:

$$U_C = \frac{a_2 U_1 + a_1 U_2}{a_2 + a_1} \tag{1}$$

and the convective Mach number is defined

$$M_C = \frac{U_C - U_2}{a_2} \tag{2}$$

The volumetric flow rates of the ethanol were $8 \pm 1$ cc/min for air and $9 \pm 1$ cc/min for helium ($6.3 \pm 0.8$ and $7.1 \pm 0.8$ g/min, respectively, at ambient conditions).

**Table 1 Main flow and injection conditions**

| Property | Units | Main flow | Helium jet | Air jet |
|---|---|---|---|---|
| Stagnation | | | | |
| $p_0$ | kPa | $793 \pm 3$ | $434 \pm 21$ | $510 \pm 28$ |
| $T_0$ | K | $290 \pm 1$ | $290 \pm 1$ | $290 \pm 1$ |
| Nozzle exit | | | | |
| $p$ | kPa | $101 \pm 1$ | $80 \pm 5$ | $115 \pm 6$ |
| $T$ | K | $161 \pm 1$ | $147 \pm 1$ | $189 \pm 1$ |
| $U$ | m/s | $508 \pm 1$ | $1213 \pm 4$ | $449 \pm 1$ |
| $M$ | — | $2.00 \pm 0.01$ | $1.70 \pm 0.01$ | $1.63 \pm 0.01$ |
| $\dot{m}$ | kg/s | $3.78 \pm 0.02$ | $0.013 \pm 0.001$ | $0.038 \pm 0.003$ |
| $Re_d$ | — | — | 199,000 | 540,000 |
| $Re \times 10^6$ | 1/m | 101 | 28 | 75 |
| $U_C$ | m/s | — | 693.0 | 480.0 |
| $M_C$ | — | — | 0.73 | 0.11 |

**Flow Visualization**

A planar Mie-scattering technique was employed to visualize the jet mixing in the supersonic flow. The fog visualization technique revealed the injected gas in the main airstream because of the large scattering cross sections of the seeding particles. The passive scalar method[21] was employed, where the droplets were first allowed to condense in the jet and then were diluted by mixing with the main airstream. Hence, the method provided a passive marker that did not affect the velocity field. The mass fraction of ethanol was about 0.003 in the air jet and about 0.01 in the helium jet. Numerical simulations by Squires and Eaton[22] demonstrate that mass fractions of less than 1% have negligible effect on turbulence quantities in isotropic turbulence, suggesting that the condensed fog does not influence the turbulence. Upstream of the injector throat, the ethanol is in vapor form. As the flow expands through the nozzle, the ethanol condenses through homogeneous nucleation, where nuclei consist of small molecular clusters of ethanol. Wegener et al.[23] investigated the condensation of ethanol in supersonic nozzles and found that at supersaturation ratios between 10 and 14, depending on the ethanol loading, the condensation process occurred rapidly (in about 50 $\mu$s), after which virtually all of the vapor was condensed. Considering the ethanol loading of this study, the condensation occurred near the nozzle's throat, at a supersaturation ratio of about 10 for helium and about 13 for air, and ended by the time the flow reached the nozzle exit. Clumpner[24] measured the ethanol droplet-number densities leaving the nozzle exit to be about $10^{12}$–$10^{13}$ cm$^{-3}$, with radii of about 50–100 Å (diameter of 0.01–0.02 $\mu$m) and with a Gaussian distribution having a standard deviation of about 8 Å (0.0008 $\mu$m). Because the experimental conditions of Clumpner[24] were similar to those of the present work, the ethanol droplets were assumed to be of comparable size. Therefore, the tracer droplets were formed within the nozzle and carried with the fuel jet into the main flow. The question of how accurately these particles follow the flow and represent its structure can be answered by analyzing the ratio of the particle aerodynamic response time to the local flow timescale, known as the Stokes number. If the ethanol droplets are assumed to have a diameter of 0.02 $\mu$m, the calculated Stokes number is about 0.0002 in the air jet and about 0.005 in the helium jet. Direct numerical simulations conducted by Samimy and Lele[25] for a particle-laden compressible mixing layer suggest that, for proper visualization, the Stokes number should be less than 0.5, where the fluid timescale is based on the vorticity thickness of the shear layer. Using the incompressible result that the visual thickness is about twice the vorticity thickness, the Stokes number based on the visual thickness should be less than 0.25. This condition is met in this study by the particles emerging from the injector exit. Farther downstream, the particles grow because of collisions and coagulation; however, the condition on the Stokes number is still met by particles 10 times larger than the estimated size. It is concluded that the visualization is correct in the sense that the particles do follow the flow.

*Spatial Resolution*

The smallest imaged area was about 28 mm (1.1 in.) $\times$ 28 mm (1.1 in.) ($\approx$780 mm$^2$) resulting in an area of 109 $\times$ 109 $\mu$m pixel. The smallest scale in the flow is the Batchelor, or mass-diffusion, scale $\lambda_B$, which follows the relation $\lambda_B \sim \delta Sc^{-1/2} Re_{\delta,\Delta U}^{-3/4}$, where $\delta$ is the local width of the shear layer (taken as the diameter of the jet), $Re_{\delta,\Delta U}$ is the local Reynolds number based on the velocity difference of the shear flow (jet centerline velocity minus the mainstream velocity) and $\delta$, and $Sc$ is the Schmidt number. The results of Dowling and Dimotakis[26] suggest a proportionality constant of about 12.5. Hence, $\lambda_B = 12.5 \times \delta Sc^{-1/2} Re_{\delta,\Delta U}^{-3/4}$. To quantify the resolution of the experiment, $L/\lambda_B$ is estimated, where $L$ is the largest dimension of the examined volume (here 109 $\mu$m). If this ratio is greater than 1, the amount of mixed fluid will be overpredicted, because both mixed and pure fluids can reside within the examined volume.[27] In the present visualization experiments, the resolution is $L/\lambda_B = 5$ for the air jet, and about 7 for the helium jet. For larger fields of view, the spatial resolution is lower.

*Temporal Resolution*

The mean Batchelor-scale passage time is calculated on the basis of Batchelor's length scale and the jet exit velocity $\tau_B = \lambda_B / U$. This timescale is about 50 ns for the air jet and 12 ns for the helium jet. The duration of the laser pulse is 10 ns, i.e., less than the Batchelor-scale passage time.

**Image Processing**

The images were analyzed on a workstation using a commercial image-processing software package.[3] Ten background images acquired with the flow off and the light sheet blocked from reaching the model were averaged. Also, 10 reference images acquired with the light sheet at the model, but with the flow off, were averaged. To remove undesirable background illumination levels and thermal currents, the average background image was subtracted from all images, including the reference images. To correct for nonuniformities in the light sheet, the images were divided by the average reference image. The cross-sectional-view images also were corrected for the view angle distortion of the camera–mirror system by spatially transforming (warping) them using a reference grid taken during the test. The transformed image looked as it would have appeared in a perpendicular imaging arrangement. Further image processing is discussed in the following section.

## Results and Discussion

Planar imaging techniques, including the Mie scattering, produce two-dimensional images containing intensity information that characterizes the flow. Because all of the images were acquired under the same flow conditions, the changes observed were caused by the different nozzle inserts and the interaction between the main flow and the ethanol-seeded jet. Mixing and jet penetration were quantified through image processing. In addition, analysis of the instantaneous images gave information about the structural behavior of the jet–mainstream interface region and qualitative characteristics of the mixing. To facilitate the interpretation of the results, length scales in centimeters are drawn, in addition to the ramp and the injector inserts, which are superimposed on each image. In the side views, the flow is from left to right, and the length scales are measured from the bottom wall and the injector exit. In the transverse views the flow comes out of page, and the length scales are measured from the bottom wall and the centerline.

**Flow Structure**

Selected instantaneous images are shown in Figs. 4–9. Side-view images of the near field on the centerline plane of all of the injectors are presented for air and helium in Figs. 4 and 5, respectively. Large-scale structures are visible in all of the images. Smaller-scale structures are also visible and appear to dominate the interface structure. No differences between the air and the helium jets are noticed, except the void in the left side of the images in Fig. 4, where the close proximity of the air jet to the injector exit, and the sudden compression, caused the re-evaporation of the ethanol downstream the barrel shock Mach disk. This feature is not observed in the helium case because the jet was almost pressure-matched to the surroundings, and therefore the shock compression was too weak to vaporize the ethanol. Instantaneous cross-section images of ethanol-seeded jets

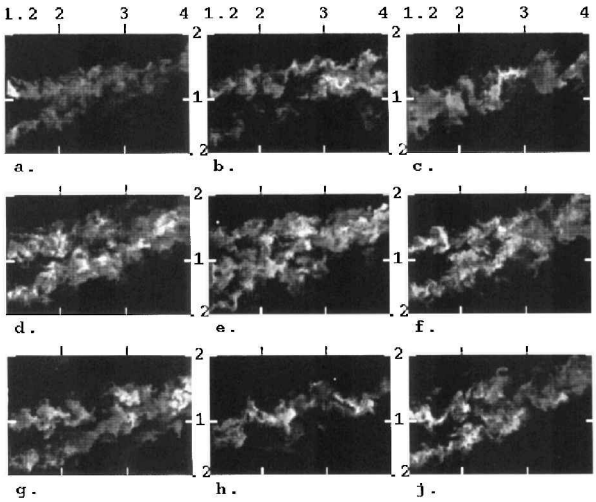


**Fig. 4 Instantaneous side-view images of ethanol-seeded air injection: a) circular, b) nozzle with steps, c) trapezoidal, d) nozzle with vortex generators in X orientation, e) tapered-slot nozzle with parallel throat, f) elliptical nozzle with parallel major axis, g) nozzle with vortex generators in cross orientation, h) tapered-slot nozzle with perpendicular throat, and j) elliptical nozzle with perpendicular major axis (length scales in centimeters).**

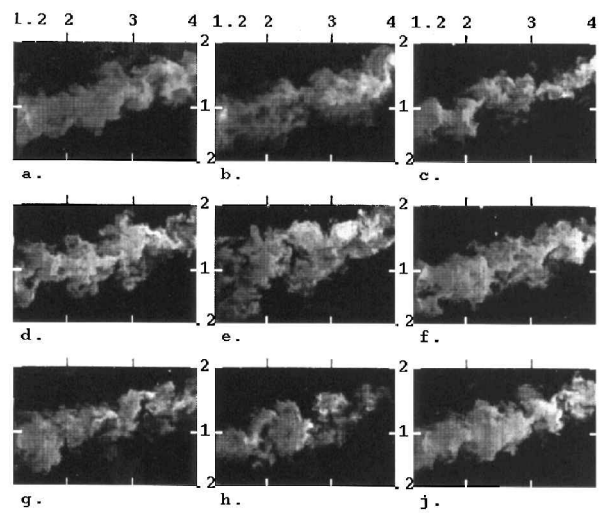


**Fig. 5 Instantaneous side-view images of ethanol-seeded helium injection: a) circular, b) nozzle with steps, c) trapezoidal, d) nozzle with vortex generators in X orientation, e) tapered-slot nozzle with parallel throat, f) elliptical nozzle with parallel major axis, g) nozzle with vortex generators in cross orientation, h) tapered-slot nozzle with perpendicular throat, and j) elliptical nozzle with perpendicular major axis (length scales in centimeters).**

of all nine configurations are shown in Figs. 6–9. Figures 6 and 7 show the transverse images at axial position $x/h = 0.75$ for air and helium jets, respectively. In the near field, each nozzle insert produces a distinctive jet. The circular nozzle and the nozzle with three steps create a circular cross-section jet. The trapezoidal insert creates a trapezoidal jet. The nozzle with the vortex generators deformed the jet, each tab creating a small indent in the jet cross section. The jet from the tapered nozzle spreads more to the minor axis of the slot, whereas the elliptical nozzle produces a jet of an elliptical cross section. The air jets show a toroidal shape in cross section, caused by the barrel shock compression and reevaporation of the ethanol, as discussed earlier. All of these images show the cross section of the jet to be similar to the cross section of the nozzle, indicating the lack of interaction between the jet and the main flow at this axial station. Cross sections of ethanol-seeded air jets are shown in Figs. 8 and 9

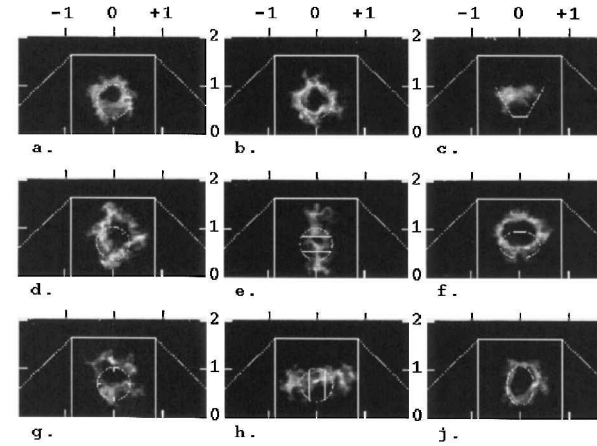


**Fig. 6 Instantaneous transverse images of ethanol-seeded air injection at $x/h = 0.75$: a) circular, b) nozzle with steps, c) trapezoidal, d) nozzle with vortex generators in X orientation, e) tapered-slot nozzle with parallel throat, f) elliptical nozzle with parallel major axis, g) nozzle with vortex generators in cross orientation, h) tapered-slot nozzle with perpendicular throat, and j) elliptical nozzle with perpendicular major axis (length scales in centimeters).**

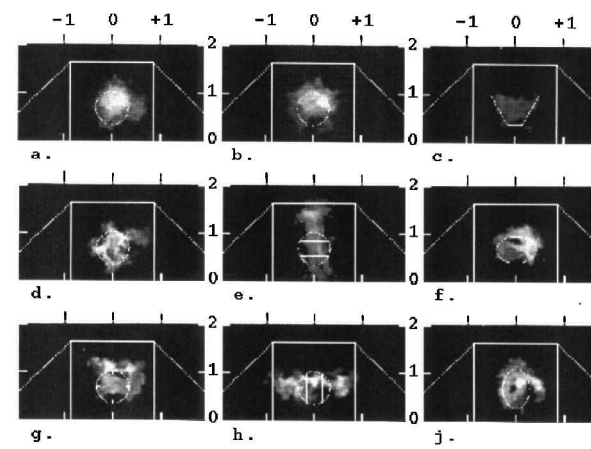


**Fig. 7 Instantaneous transverse images of ethanol-seeded helium injection at $x/h = 0.75$: a) circular, b) nozzle with steps, c) trapezoidal, d) nozzle with vortex generators in X orientation, e) tapered-slot nozzle with parallel throat, f) elliptical nozzle with parallel major axis, g) nozzle with vortex generators in cross orientation, h) tapered-slot nozzle with perpendicular throat, and j) elliptical nozzle with perpendicular major axis (length scales in centimeters).**

for $x/h = 3.9$ and 7, respectively. In Fig. 8, at $x/h = 3.9$, all of the images exhibit a horseshoe shape caused by the ramp-generated vortices that stretch the jet and draw air from the mainstream into the jet core. Farther downstream, in Fig. 9 at $x/h = 7$, the jet becomes independent of the injection geometry and displays a quasicircular pattern with a slight dip in the bottom of the jet cross section, reminiscent of the horseshoe shape. In this region, the vortices draw from the upper part of the fuel jet into the core, refilling it. Both large-scale and small-scale structures are visible in all images. In cross section, the helium jets (not shown) display the same flow features as the air jets.[3]

### Mixing Characterization

A variety of structures were observed over the ensemble of images acquired in each case. Because it is possible to support almost any hypothesis concerning the mixing process by preferential consideration of only those images displaying the desired features, it is desirable to have a more objective tool for the analysis of predominant structure size and orientation. For this reason, this investigation made use of composite images instead of instantaneous ones.

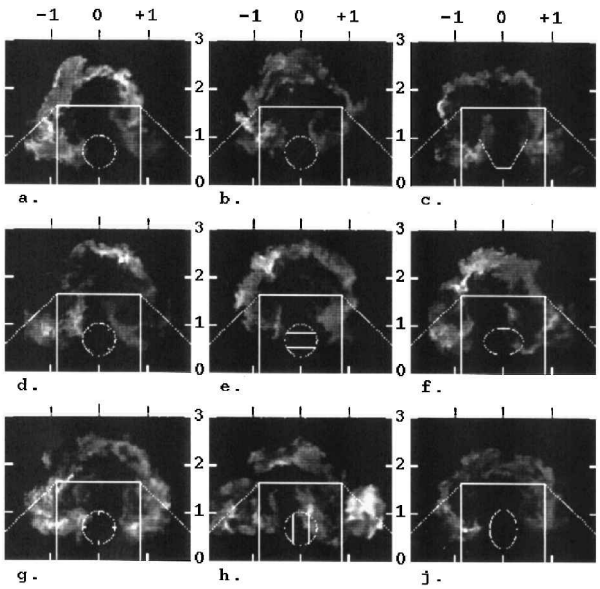


**Fig. 8 Instantaneous transverse images of ethanol-seeded air injection at $x/h$ = 3.9: a) circular, b) nozzle with steps, c) trapezoidal, d) nozzle with vortex generators in X orientation, e) tapered-slot nozzle with parallel throat, f) elliptical nozzle with parallel major axis, g) nozzle with vortex generators in cross orientation, h) tapered-slot nozzle with perpendicular throat, and j) elliptical nozzle with perpendicular major axis (length scales in centimeters).**

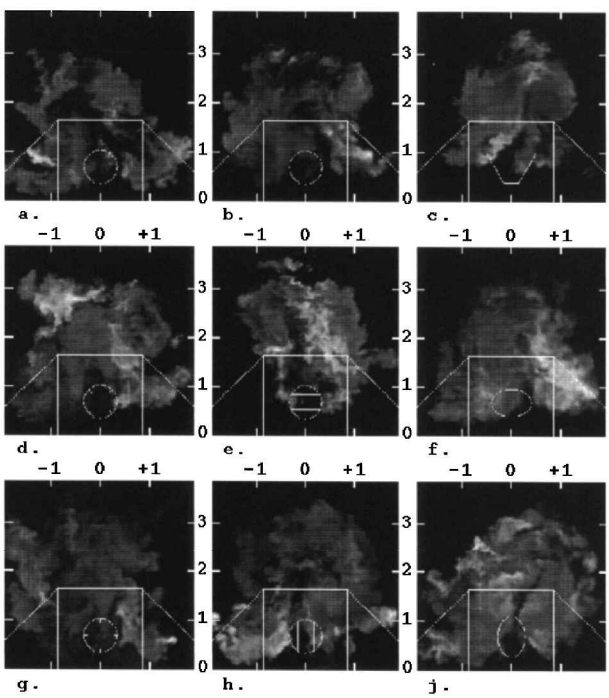


**Fig. 9 Instantaneous transverse images of ethanol-seeded air injection at $x/h$ = 7: a) circular, b) nozzle with steps, c) trapezoidal, d) nozzle with vortex generators in X orientation, e) tapered-slot nozzle with parallel throat, f) elliptical nozzle with parallel major axis, g) nozzle with vortex generators in cross orientation, h) tapered-slot nozzle with perpendicular throat, and j) elliptical nozzle with perpendicular major axis (length scales in centimeters).**

Compositing images is a technique that is often used with CCD cameras. Instead of taking a long exposure, a number of shorter exposures are taken and subsequently summed to the equivalent of a long-exposure image. In a composite image the noise level is low because of its lack of correlation from one image to another, whereas the useful (repetitive) signals add up. In the present case, 10 images are composited, increasing the signal-to-noise ratio by a factor of $\sqrt{10}$ relative to a single image of equivalent duration. The composite image was first scaled to 8-bit representation, i.e., from zero (black) to 255 (white), and then thresholded, thus dividing it into two distinct regions—the background and the foreground—representing the ethanol-seeded region. A careful inspection of the visual information contained throughout this scale, suggested that a uniform threshold of 55 was the most suitable value for the presentation and evaluation of the data of current interest. Threshold values lower than 10 resulted in a quasi circular object with very little detail on the perimeter. Threshold values greater than 100 caused the loss of the jet shape and edges. Values between 30 and 80 did not change the object properties calculated after the thresholding. Deviations in the geometric properties also were observed for intermediate values between 10–30 and 80–100. Therefore, judging from the good signal-to-noise ratios and well-defined edges, it was concluded that the information on the images was relatively insensitive to the threshold value between 30 and 80. Following the image thresholding, several geometric properties related to mixing were computed. Mixing is a two-step process in which the stretching, through its gradient intensification, is a necessary precursor to diffusion. Because all of the jets were produced under the same conditions (temperature, pressure, area ratio), the jet with more stretching also produces better small-scale mixing (the improved small-scale mixing being caused by the enhanced stretching, and not by a change in the flow conditions). Because the jet stretching is macroscaled, it can be characterized through the geometric properties of its cross section, in particular, the cross-sectional area and the perimeter. The growth of the cross-sectional area is proportional to the amount of the surrounding air, which is entrained by the macromixing, whereas the perimeter is a measure of the jet distortion and stretching; more stretching causing longer and more convoluted perimeters. An additional factor, compactness $[=(\text{perimeter})^2/(4\pi\text{area})]$ is used to characterize the effectiveness of the various nozzle inserts. Higher compactness values indicate longer and more convoluted interfaces that facilitate molecular-scale mixing through diffusion. The $z$ centroid of the thresholded image also was calculated, to provide an indication for the jet penetration.

Four cross-sectional composite images of the slot-throat nozzle with the horizontal slot are presented in Fig. 10, whereas Fig. 11 shows the four cross-sectional composite images of the slot-throat nozzle with the vertical slot. The contour representing the threshold value also is plotted on the images. These figures illustrate

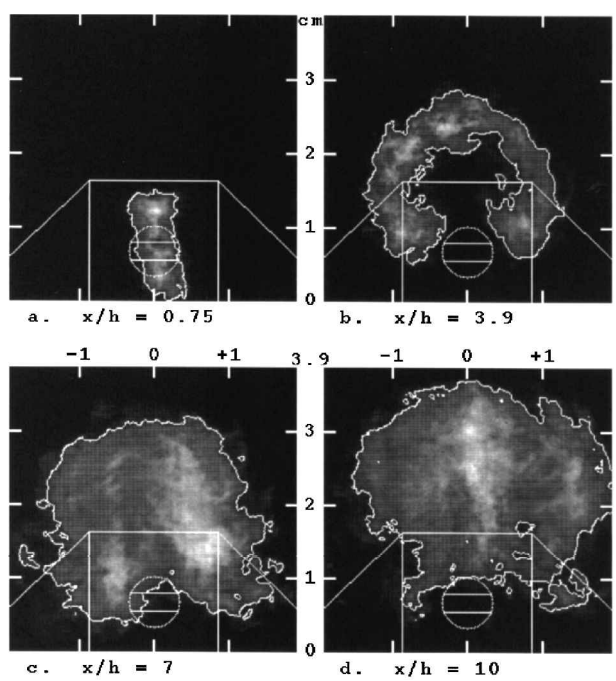


**Fig. 10 Composite images of ethanol-seeded air injection from tapered-slot nozzle with parallel throat.**

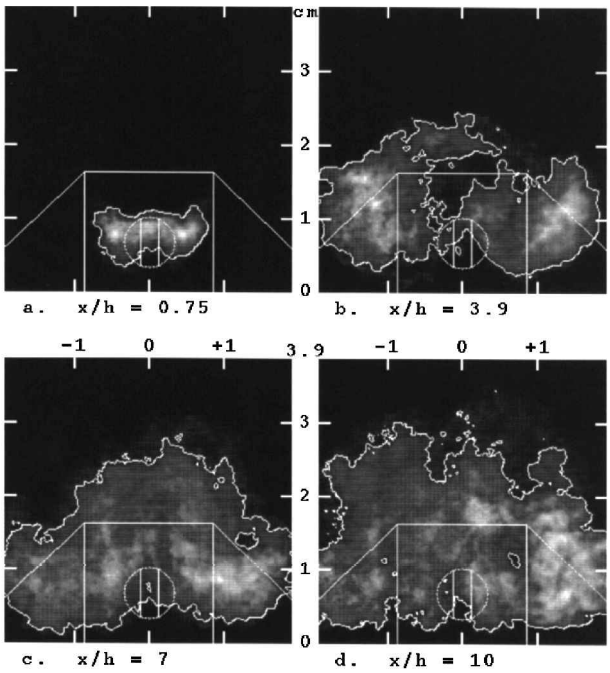


**Fig. 11 Composite images of ethanol-seeded air injection from tapered-slot nozzle with perpendicular throat.**

the coupling between the vorticity generated by the ramp and the preconditioned jet. For $x/h = 3.9$, Fig. 10 displays a circular and coherent horseshoe. At the same cross section, Fig. 11 displays a laterally stretched jet that is almost split into two separate blobs. The only difference between these figures is the throat orientation: In Fig. 10, the slot is parallel to the bottom wall, whereas in Fig. 11, it is perpendicular to the bottom wall.

The normalized cross-sectional area of the air jets is displayed in Fig. 12a. The area increases monotonously downstream, up to $x/h = 7$. Beyond this point the area remains constant for all of the inserts with the exception of the vertical tapered throat, which continues to grow. The normalized perimeter shown in Fig. 12b increases at a higher rate for $x/h < 3.9$ than for $x/h \geq 3.9$. The increased perimeter for a constant area in these two planes suggests that the interface is more convoluted in the downstream plane than in the upstream plane. This conclusion is supported by Fig. 12c, where the compactness factor increases from $x/h = 7$ to 10, indicating mixing enhancement. The compactness factor increases rapidly for $x/h < 3.9$, caused by the rapid stretching in the near field of the jet by the applied vorticity. This stretching increases the perimeter length, while the area (which is proportional to the mass entrainment) grows slowly, the combined effect producing a very high compactness. For $x/h \geq 3.9$, the area starts growing faster (because the vortical flow draws fuel from the upper part of the jet into the jet core), thus refilling the jet with fuel, slowing the interface growth, and consequently decreasing the compactness factor. The refilling of the jet core causes the $z$ centroid, displayed in Fig. 12d, to increase monotonously downstream at an angle of about 8 deg for $x/h < 3.9$, and at an angle of about 5 deg for $x/h > 3.9$. The perpendicular tapered-throat nozzle produces a lower jet penetration because it spreads more laterally than perpendicularly to the wall, thus lowering the area's centroid. Because the tapered nozzle with the perpendicular slot spreads more laterally than the other inserts, the spread of this jet exceeds the field of view for cross sections $x/h = 7$ and 10 (Figs. 11c and 11d, respectively), introducing errors in the calculation of the area, perimeter, and compactness. Hence, the calculated area and perimeter length for this nozzle are smaller than the actual values.

Each area, perimeter, and centroid point in Fig. 12 was deduced from a set of 4 images, composited of 10 shots each, indicating a repeatability of better than $\pm 5\%$ relative to the mean.

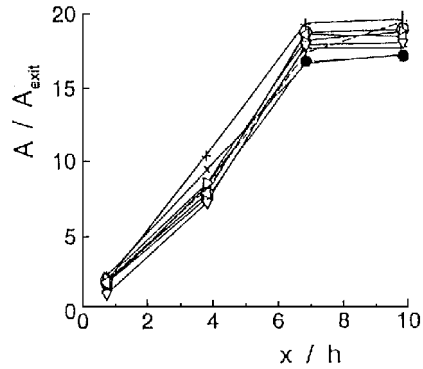


**a) Normalized jet area**

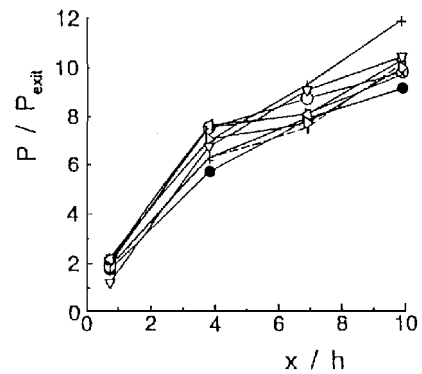


**b) Normalized jet perimeter**

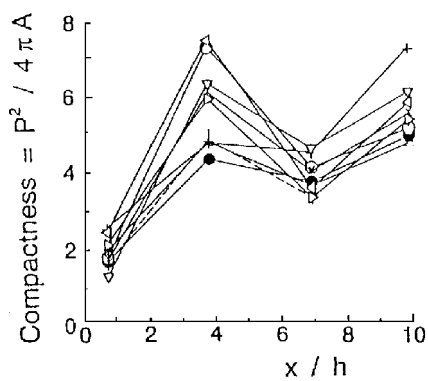


**c) Jets cross-section compactness**

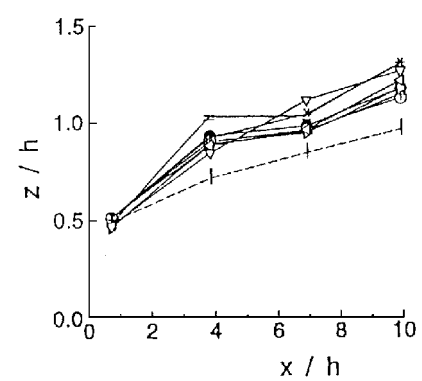


**d) Normalized *z*-centroid**

**Fig. 12 Jet mixing characteristics: ●circular; ♂ nozzle with steps; ▽trapezoidal; ×, nozzle with vortex generators in X orientation; +, nozzle with vortex generators in cross orientation; =, tapered-slot nozzle with parallel throat; |, tapered-slot nozzle with perpendicular throat; ▷, elliptical nozzle with parallel major axis; and ◁, elliptical nozzle with perpendicular major axis.**

## Summary and Conclusions

An experimental investigation of the effects of internal nozzle geometry on compression-ramp mixing in supersonic flows was conducted using planar Mie scattering for flow visualization. This technique, which is simple and safe to use, allowed direct observation of the mixing process between a supersonic main flow over a swept-ramp injector and a preconditioned supersonic jet. The results obtained from four cross planes and one side view of the flow provided a clear identification of the jet–mainstream interface. Because supersonic mixing is independent of the molecular weight of the injected gas, air can be substituted for expensive helium in investigations of nonreacting flows. An image-processing method for the extraction of geometric information in terms of area, perimeter, and centroid is used to analyze mixing and penetration, and to compare different injector inserts. To test different jet precondition schemes, six nozzle inserts (in nine configurations) were used. The results indicate, however, that the flow is dominated by the strong vortical flow generated by the swept ramp. The coupling effect between the preconditioned jet and the vortical flow is weak, but still has the potential of enhancing the near-field mixing. All nozzle inserts have a better mixing performance relative to the circular-nozzle baseline configuration, demonstrating that the coupling effect does enhance mixing. The minor differences noticed among the various fuel-nozzle jets indicate that the injected mixing at $x/h > 7$ downstream of the injectors is nearly independent of jet geometry, injected molecular weight, and shear level or initial convective Mach number. At $x/h = 10$, the nozzle with the vortex generators in "cross orientation" produces the largest perimeter length together with the largest area and compactness, indicating its enhanced mixing characteristics compared to the other inserts. At this station, the jet of the perpendicular slot-throat nozzle spread out of the field of view, and therefore its characterization is not accurate. This jet, which appears to have a significant mixing potential, spreads laterally and is captured by the two ramp-generated vortices, which further stretch the jet sideways, almost splitting it into two separate jets. This behavior improves the near-field mixing by increasing the interface between the jet and the main flow.

The slot-throat nozzle and the nozzle with vortex generators emerge as the most promising candidates for swept-ramp scramjet injectors.

## Acknowledgments

This work was supported through NASA Grant NAS1-19858, Task 4, NASA Langley Research Center. Thanks to Andrew D. Cutler, Donna K. Kraus, and Clinton J. Reese for their support and assistance.

## References

[1]Papamoschou, D., and Roshko, A., "The Compressible Turbulent Shear Layer: An Experimental Study," *Journal of Fluid Mechanics*, Vol. 197, Dec. 1988, pp. 453–477.

[2]Billig, F. S., "Research on Supersonic Combustion," AIAA Paper 92-0001, Jan. 1992.

[3]Haimovitch, Y., Gartenberg, E., and Roberts, A. S., Jr., "Investigation of Ramp Injectors for Supersonic Mixing Enhancement," NASA-CR-4634, Nov. 1994.

[4]Northam, G. B., Greenberg, I., and Byington, C. S., "Evaluation of Parallel Injector Configurations for Supersonic Combustion," AIAA Paper 89-2525, July 1989.

[5]Northam, G. B., Capriotti, D. P., Byington, C. S., and Greenberg, I., "Mach 2 and Mach 3 Mixing and Combustion in Scramjets," AIAA Paper 91-2394, June 1991.

[6]Riggins, D. W., Mekkes, G. L., McClinton, C. R., and Drummond, J. P., "A Numerical Study of Mixing Enhancement in a Supersonic Combustor," AIAA Paper 90-0203, Jan. 1990.

[7]Riggins, D. W., and McClinton, C. R., "A Computational Investigation of Flow Losses in a Supersonic Combustor," AIAA Paper 90-2093, July 1990.

[8]Riggins, D. W., and McClinton, C. R., "Analysis of Losses in Supersonic Mixing and Reacting Flows," AIAA Paper 91-2266, June 1991.

[9]Davis, D. O., and Hingst, W. R., "Progress Towards Synergistic Hypermixing Nozzles," AIAA Paper 91-2264, June 1991.

[10]Hartfield, R. J., Jr., Hollo, S. D., and McDaniel, J. C., "Experimental Investigation of a Supersonic Swept Ramp Injector Using Laser Induced Iodine Fluorescence," AIAA Paper 90-1518, June 1990.

[11]Donohue, J. M., Haj-Hariri, H., and McDaniel, J. C., "Vorticity Generation Mechanisms in Parallel Injection Schemes for Supersonic Mixing," AIAA Paper 92-3286, July 1992.

[12]Donohue, J. M., McDaniel, J. C., and Haj-Hariri, H., "Experimental and Numerical Study of Swept Ramp Injection into a Supersonic Flow Field," AIAA Paper 93-2445, June 1993.

[13]Gutmark, E., Schadow, K. C., and Wilson, K. J., "Noncircular Jet Dynamics in Supersonic Combustion," *Journal of Propulsion and Power*, Vol. 5, No. 5, 1989, pp. 529–533.

[14]Gutmark, E., Schadow, K. C., and Wilson, K. J., "Subsonic and Supersonic Combustion Using Noncircular Injectors," *Journal of Propulsion and Power*, Vol. 7, No. 2, 1991, pp. 240–249.

[15]Schadow, K. C., Gutmark, E., Parr, T. P., Parr, D. M., and Wilson, K. J., "Enhancement of Fine Scale Mixing for Fuel Rich Plume Combustion," AIAA Paper 87-0376, Jan. 1987.

[16]Samimy, M., Reeder, M., and Zaman, K. B. M. Q., "Supersonic Jet Mixing Enhancement by Vortex Generations," AIAA Paper 91-2263, June 1991.

[17]Samimy, M., Zaman, K. B. M. Q., and Reeder, M., "Effect of Tabs on the Flow and Noise Field of an Axisymmetric Jet," *AIAA Journal*, Vol. 31, No. 4, 1993, pp. 609–619.

[18]Zaman, K. B. M. Q., Reeder, M. F., and Samimy, M., "Supersonic Jet Mixing Enhancement by Delta-Tabs," AIAA Paper 92-3548, July 1992.

[19]Gutmark, E., Bowman, H. L., and Schadow, K. C., "Flow and Acoustic Features of a Supersonic Tapered Nozzle," *Experiments in Fluids*, Vol. 13, No. 1, 1992, pp. 49–55.

[20]Cutler, A. D., Levey, B. S., and Kraus, D. K., "An Experimental Investigation of Supersonic Swirling Jets," AIAA Paper 93-2922, July 1993.

[21]Clemens, N. T., and Mungal, M. G., "A Planar MIE Scattering Technique for Visualizing Supersonic Mixing Flows," *Experiments in Fluids*, Vol. 11, No. 2/3, 1991, pp. 175–185.

[22]Squires, K. D., and Eaton, J. K., "Particle Response and Turbulence Modification in Isotropic Turbulence," *Physics of Fluids A*, Vol. 2, No. 7, 1990, pp. 1191–1203.

[23]Wegener, P. P., Clumpner, J. A., and Wu, B. J. C., "Homogeneous Nucleation and Growth of Ethanol Drops in Supersonic Flow," *Physics of Fluids*, Vol. 15, No. 11, 1972, pp. 1869–1876.

[24]Clumpner, J. A., "Light Scattering from Ethyl Alcohol Droplets Formed by Homogeneous Nucleation," *Journal of Chemical Physics*, Vol. 55, No. 10, 1971, pp. 5042–5045.

[25]Samimy, M., and Lele, S. K., "Particle-Laden Compressible Free Shear Layers," AIAA Paper 90-1977, July 1990.

[26]Dowling, D. R., and Dimotakis, P. E., "Similarity of the Concentration Field of Gas-Phase Turbulent Jets," *Journal of Fluid Mechanics*, Vol. 218, 1990, pp. 109–142.

[27]Clemens, N. T., Paul, P. H., Mungal, M. G., and Hanson, R. K., "Scalar Mixing in the Supersonic Shear Layer," AIAA Paper 91-1720, June 1991.

F. W. Chambers
*Associate Editor*